

Multi-Wavelength Studies of the Optically Dark Gamma-Ray Burst 001025A

K. Pedersen,¹ K. Hurley,² J. Hjorth,¹ D. A. Smith,³ M. I. Andersen,⁴ L. Christensen,⁴ T. Cline,⁵ J. P. U. Fynbo,¹ J. Goldsten,⁶ S. Golenetskii,⁷ J. Gorosabel,⁸ P. Jakobsson,¹ B. L. Jensen,¹ B. Milvang-Jensen,⁹ T. McClanahan,⁵ P. Møller,¹⁰ V. Palshin,⁷ N. Schartel,¹¹ J. Trombka,⁵ M. Ulanov,⁷ D. Watson¹

ABSTRACT

We identify the fading X-ray afterglow of GRB 001025A from *XMM-Newton* observations obtained 1.9–2.3 days, 2 years, and 2.5 years after the burst. The non-detection of an optical counterpart to an upper limit of $R = 25.5$, 1.20 days after the burst, makes GRB 001025A a “dark” burst. Based on the X-ray afterglow spectral properties of GRB 001025A, we argue that some bursts appear

¹Dark Cosmology Centre, Niels Bohr Institute, University of Copenhagen, Juliane Maries Vej 30, DK-2100 Copenhagen Ø, Denmark; kp, jens, jfynbo, pallja, brian_j, darach @astro.ku.dk

²Space Sciences Laboratory, 7 Gauss Way, University of California, Berkeley, CA 94720-7450, USA; khurley@ssl.berkeley.edu

³NSF Postdoctoral Fellow, University of Michigan, Department of Physics Ann Arbor, MI 48109, USA; donaldas@umich.edu

⁴Astrophysikalisches Institut Potsdam, An der Sternwarte 16, 14482 Potsdam, Germany; mandersen, lchristensen @aip.de

⁵NASA Goddard Space Flight Center Code 661 Greenbelt, MD 20771, USA; Thomas.L.Cline, Timothy.P.McClanahan, Jacob.I.Trombka.1 @nasa.gov

⁶The Johns Hopkins University Applied Physics Laboratory Laurel, MD 20723, USA; john.goldsten@jhuapl.edu

⁷Ioffe Physico-Technical Institute, St. Petersburg, 194021, Russia; golen, val, mulanov @mail.ioffe.ru

⁸IAA-CSIC, P.O. Box 03004, 18080 Granada, Spain and Space Telescope Science Institute, 3700 San Martin Drive, Baltimore, MD21218, USA; jgu@laeff.esa.es

⁹Max-Planck-Institut für extraterrestrische Physik, Giessenbachstr., D-85748 Garching; milvang@mpe.mpg.de

¹⁰European Southern Observatory, Karl Schwarzschild-Strasse 2, D-85748 Garching bei München, Germany; pmoller@eso.org

¹¹*XMM-Newton* Science Operations Centre, ESA, Villafranca del Castillo, P.O. Box 50727, 28080 Madrid, Spain; nscharte@xmm.vilspa.esa.es

optically dark because their afterglow is faint and their cooling frequency is close to the X-ray band. This interpretation is applicable to several of the few other dark bursts where the X-ray spectral index has been measured. The X-ray afterglow flux of GRB 001025A is an order of magnitude lower than for typical long-duration gamma-ray bursts. The spectrum of the X-ray afterglow can be fitted with an absorbed synchrotron emission model, an absorbed thermal plasma model, or a combination thereof. For the latter, an extrapolation to optical wavelengths can be reconciled with the R -band upper limit on the afterglow, without invoking any optical circumburst absorption, provided the cooling frequency is close to the X-ray band. Alternatively, if the X-ray afterglow is due to synchrotron emission only, seven magnitudes of extinction in the observed R -band is required to meet the R -band upper limit, making GRB 001025A much more obscured than bursts with detected optical afterglows. Based on the column density of X-ray absorbing circumburst matter, an SMC gas-to-dust ratio is insufficient to produce this amount of extinction. The X-ray tail of the prompt emission enters a steep temporal decay excluding that the tail of the prompt emission is the onset of the afterglow. To within the astrometric uncertainty, this afterglow was coincident with an extended object, seen in a deep VLT R -band image, which we identify as the likely host galaxy of GRB 001025A.

Subject headings: gamma rays: bursts — X-rays: general

1. INTRODUCTION

One of the enduring mysteries of cosmic gamma-ray bursts (GRBs) is that of the so-called “dark” bursts - those with no detected optical or near-infrared afterglows. In the fireball model of GRBs (for a review, see Meszaros 2002), an explosive event produces a relativistically expanding blast wave. Internal shocks within the blast wave are the source of the high energy prompt emission while afterglows arise from external shocks when the blast wave run into an interstellar medium.

GRBs may be divided into “long-duration” and “short-duration” categories; no unambiguous detection of an optical afterglow has yet been made for any short-duration event (e.g. Bloom et al. 2005; Hjorth et al. 2005; Gorosabel et al. 2002; Hurley et al. 2002) and only in one case has an X-ray afterglow been detected (Gehrels et al. 2005). On the other hand, virtually all of the long-duration bursts display fading soft X-ray afterglows (e.g. Costa 1999; De Pasquale et al. 2003), and they have been shown to be associated with supernova explosions (Hjorth et al. 2003b; Stanek et al. 2003; Malesani et al. 2004).

For more than half of the long-duration GRBs no optical and/or radio afterglow has been detected (e.g. Fynbo et al. 2001; Lazzati et al. 2002; Berger et al. 2002); however, rapid and systematic follow-up of bursts has decreased the relative fraction of dark bursts in recent years (Rol et al. 2005; Berger et al. 2005). Recently, Jakobsson et al. (2004) suggested using the value of the optical-to-X-ray spectral index as a diagnostic for early identification of dark bursts, and they found five dark bursts (including GRB 001025A) in their sample of 52 bursts.

There are several possible explanations for dark bursts (Fynbo et al. 2001). They could be at very high redshifts (Lamb & Reichart 2000), or they could be heavily obscured by dust in their host galaxies (e.g. Groot et al. 1998; Taylor et al. 1998; Reichart & Price 2002). They could also occur in regions where the surrounding medium is tenuous, far from the centers of their host galaxies, where the strong shocks required for particle acceleration could not form (Kumar & Panaitescu 2000).

Observations of bursts detected by the *BeppoSAX*, the *High Energy Transient Explorer*, and the *Rossi X-ray Timing Explorer* spacecrafts have indeed shown that bursts can be dark for a variety of reasons. Some bursts seem in fact to be dark due to extinction, e.g. GRB 000210 (Piro et al. 2002), GRB 970828 (Djorgovski et al. 2001), and GRB 001109 (Castro Cerón et al. 2004). Other bursts have faint optical afterglows either because of moderately high redshift, e.g., GRB 020124 (Hjorth et al. 2003a; Berger et al. 2002), or because they are intrinsically faint without extinction, e.g. GRB 980613 (Hjorth et al. 2002) and GRB 021211 (Crew et al. 2003). Analysis of bursts detected by *Swift* will undoubtedly shed more light on the nature of dark bursts. Already now it has become evident that afterglows of bursts detected by *Swift* on average are fainter than afterglows from bursts detected by previous instruments (1.7 magnitudes in the optical/near-infrared (Berger et al., 2005) and a factor three in X-rays Jakobsson, 2005). The rapid fading of some *Swift* bursts demonstrates that at least these become intrinsically faint after the first few hundred seconds (Tagliaferri et al. 2003).

Here we examine the case of the dark burst GRB 001025A. We report on our temporal and spectral analysis of the prompt emission, on our very deep optical upper limits on the afterglow, and on the results of our temporal and spectral analysis of the X-ray afterglow. Finally, we discuss the nature of GRB 001025A within the framework of the fireball model, and the implications for dark bursts in general.

2. OBSERVATIONS

2.1. GRB 001025A Prompt Emission

GRB 001025A was first reported as an event detected by the *Rossi X-Ray Transient Explorer* (RXTE) All Sky Monitor (ASM) at 11405 s UT October 25, 2000 (Smith et al. 2000). Its duration in the ASM 1.5–12 keV energy band was ~ 15 s, and its peak flux was ~ 4 Crab (10^{-7} erg cm $^{-2}$ s $^{-1}$) in the 5–12 keV band. The event was detected by a single camera and localized to a $4' \times 1.6'$ error box. It was also observed by *Ulysses*, the X-Ray/Gamma-Ray Spectrometer (XGRS) aboard the *Near Earth Asteroid Rendezvous* mission (NEAR), and *Wind* (Konus experiment) in the Interplanetary Network (IPN), and triangulated to a preliminary $5.6'$ wide annulus which crossed the ASM error box to form a 25 arcminute 2 error box (Hurley, Cline & Smith 2000; Hurley 2000).

We have used the final *Ulysses*, NEAR, and *Wind*-Konus data to obtain a refined IPN error box for this burst. The *Ulysses* - Konus annulus is centered at R.A.(2000) = $169^{\circ}8656$, decl.(2000) = $-56^{\circ}6466$, and has a radius of $53^{\circ}5052 \pm 0^{\circ}0073$ (3σ). The *Ulysses* - NEAR annulus is centered at R.A.(2000) = $145^{\circ}4502$, decl.(2000) = $-36^{\circ}9464$, and has a radius of $27^{\circ}9969 \pm 0^{\circ}0275$ (3σ). The intersection of these annuli defines a 96 arcminute 2 error box. However, the intersection of the *Ulysses*-Konus annulus with the ASM error box defines a 3.3 arcminute 2 error box, whose coordinates are given in Table 1. The combined ASM-IPN error box is shown in Figure 5.

The ASM, Konus, and XGRS lightcurves are shown in Figure 1. With a T_{90} duration of 2.9 s (i.e., the time to accumulate between 5% and 95% of the photons) in the 50–200 keV energy range, this burst falls into the “long-duration” category. Figure 1 shows the lightcurve in several energy ranges, and indicates the intervals used for time-resolved spectral analysis. This figure also shows the hardness ratio as a function of time. A hard-to-soft evolution, which is often observed in GRBs (e.g. Preece et al. 1998), is evident. The energy spectra are presented in Figure 2. The Band (Band et al. 1993) model, which consists of two smoothly joined power laws, was used to perform spectral fits. The Band function is:

$$f(E) = \begin{cases} A(E/100)^{\alpha} \exp(-E/E_0) & \text{if } E < (\alpha - \beta)E_0 \\ A\{(\alpha - \beta)E_0/(100)\}^{(\alpha-\beta)} \exp(\beta - \alpha)(E/100)^{\beta} & \text{if } E \geq (\alpha - \beta)E_0 \end{cases} \quad (1)$$

This yields a peak energy in the range $E_0 \sim 85 - 140$ keV during the burst (see Table 2). The 15–2000 keV peak flux of this burst was 3.3×10^{-5} erg cm $^{-2}$ s $^{-1}$ over 0.048 s, and the 15–2000 keV fluence was 1.3×10^{-5} erg cm $^{-2}$. Neither the time history, nor the spectrum, nor the intensity of this event was exceptional in any way. Atteia (2003) has proposed a simple

redshift estimator based on the photon flux, energy spectrum, and duration of a GRB. Using this method, we obtain $z \approx 0.8$, with a statistical uncertainty of about 50%.

2.2. Afterglow Searches

In the weeks immediately following GRB 001025A, optical, X-ray, and radio observations were carried out in attempts to identify an afterglow.

An optical afterglow was not identified, either in observations starting 1.16 days after the burst (Fynbo et al. 2000, $R > 22.5$), or in observations starting 1.66 days after the burst (Uemura et al. 2000, $R > 18.0$).

An *XMM-Newton* observation ~ 2 days after the burst revealed one apparently fading source (S1, see Figure 5) in the initial ASM/IPN error box (Altieri et al. 2000a). In late-time follow-up *XMM-Newton* observations this source had disappeared, strongly indicating that (S1) is the X-ray afterglow of GRB 001025A.

Radio observations with the *Very Large Array* (VLA) were carried out at two epochs, but they did not reveal any radio afterglow. The first VLA observation took place November 1, 2000, approximately 6 days after the GRB (D. Frail 2003, private communication). Unfortunately, the *XMM-Newton* attitude was subsequently revised (Altieri et al. 2000b), and the refined position of S1 was $\sim 2'$ from the initial one. Due to the off-set between the VLA pointing and the revised position of S1, the VLA sensitivity at the position of S1 was relatively low. VLA observations took place again on November 21 and 24, 2000 (27–30 days after the burst), but given the timescales and sensitivities ($\sim 200\mu\text{Jy}$) most GRB radio afterglows would not have been detected. Thus it is not clear whether this burst was radio-quiet.

In the following three sections, we present our analysis and results of optical observations and X-ray observations of the GRB 001025A afterglow.

2.3. Optical Observations with the VLT

The field of GRB 001025A was observed at the *Very Large Telescope* (VLT) equipped with the FORS1 camera at three epochs, under photometric and good seeing conditions (see Table 3 for details). The first epoch was a few hours after the release of the IPN error box (Hurley et al. 2000), the second epoch was 24 hours later, and the final epoch was 5 months later.

By comparing the combined R -band images of the three epochs we find no transient sources in the IPN error box and in particular near the *XMM-Newton* error circle of S1 to a 3σ detection limit of $R = 25.5$. Figure 3 shows a 12×12 arcsec² section of the last epoch VLT image with the *XMM-Newton* 2σ error circle overplotted. The 2σ error circle is consistent with the eastern part of what seems to be either a galaxy with two main components or a random projection of two unrelated objects. Following Piro et al. (2002), we estimate that the probability for a chance alignment is less than 1%, so we consider this object the likely host galaxy of GRB 001025A. The total magnitude of this complex is $R = 24.01 \pm 0.04$ and $B = 25.13 \pm 0.12$ (corrected for a modest foreground extinction of $E(B - V) = 0.07$?).

GRB afterglows display a wide variety of fading behaviors (see Figure 4). Of the *Swift* detected optical afterglows, all but GRB 030115 would have been detected in the VLT observations. The failure to detect the optical afterglow of GRB 001025A is thus not because our observations are less sensitive than studies of other detected GRB afterglows.

2.4. X-ray Observations with *XMM-Newton*

XMM-Newton carried out observations of the region around the error box at three different epochs, spanning 1.9–2.3 days, 761.0–761.2 days, and 910.2–910.4 days after the GRB (see Table 4). The *XMM-Newton* target of opportunity observation ~ 2 days after the burst revealed at least four X-ray sources in the initial ASM/IPN error box (Altieri et al. 2000a), one of which (S1) appeared to be fading. As shown in Figure 5, only S1 is in the final ASM/IPN error box. This, along with marginal evidence for a fading behavior (see Section 4 below, and Watson et al. 2002), suggested that it was the X-ray afterglow of GRB 001025A. In order to determine with certainty whether S1 was indeed the fading afterglow (as opposed to a random, variable X-ray source such as an active galactic nucleus), we carried out a follow-up *XMM-Newton* observation. This observation started on November 25, 2002, but had to be terminated because of high background radiation; it was completed on April 23, 2003.

The first observation has already been reported on in Watson et al. (2002), but for the analysis presented here, we have made two improvements: we have omitted data taken during periods with high background, and we have analyzed data from the second and third epochs as well. The effective EPIC pn exposure times of the three *XMM-Newton* observations, after screening out high background intervals, are 15 ks, 9 ks, and 18 ks respectively.

The data were processed and analysed with SAS version 5.4.1 and XSPEC version 11.3. Periods with flares were identified based on the 10–12 keV lightcurve of the full EPIC detector and events registered during these periods (where the pn count rate was above 1.5

counts/s, and where the MOS count rate was above 0.25 counts/s) were filtered out. For the pn detector, single and double events were included in the analysis and the two exposures taken in the first epoch were co-added. For the MOS detectors, single, double, triple, and quadruple events were included in the analysis and the two MOS data sets for each epoch were co-added. pn events in the energy interval 0.3–9 keV and MOS events in the energy interval 0.4–7 keV were included in the analysis. Spectra and lightcurves of sources were extracted using a circular aperture of radius $18''$. Background events were extracted from an annulus centered on the source in question with an inner radius of $18''$ and an outer radius of $50''$. The background regions are entirely on the same chip as the relevant sources, and they do not include other contaminating sources.

Below we present results from our analysis of the *XMM-Newton* images, lightcurves, and spectra of the GRB 001025A X-ray afterglow.

2.4.1. Imaging

In the first epoch observation two sources were detected, S1 R.A.(2000)= $8^h36^m35^s.93$, decl.(2000)= $-13^\circ04'10''.82$, $\pm 0''.3$), and S2, in and in the vicinity of the final ASM/IPN error box, respectively (see Figure 5). Over the first *XMM-Newton* observation 264 net counts (0.3–12 keV) were detected for source S1 by the pn detector, corresponding to a flux of $(6.4 \pm 0.2) \times 10^{-14}$ erg cm $^{-2}$ s $^{-1}$. For source S2, 78 net counts (0.3–12 keV) were detected, corresponding to a flux of $(2.0 \pm 0.4) \times 10^{-14}$ erg cm $^{-2}$ s $^{-1}$. By the time of the second epoch observation, S1 had faded beyond detection ($f_X(0.3\text{--}12\text{ keV}) < 6 \times 10^{-15}$ erg cm $^{-2}$ s $^{-1}$) while the flux of S2 was consistent with that of the first epoch. In the third epoch observation S1 was still undetectable ($f_X(0.3\text{--}12\text{ keV}) < 5 \times 10^{-15}$ erg cm $^{-2}$ s $^{-1}$) and the flux of S2 was consistent with the flux at the first two epochs. Hence, source S2 is persistent over several years, displaying flux variations less than about 25% from epoch to epoch. S2 is coincident with an $R \sim 20$ optical source which based on a spectrum obtained with the *Nordic Optical Telescope* seems to be a QSO at redshift $z \approx 2.5$ (M. I. Andersen, private communication).

2.4.2. Lightcurve

The pn lightcurve for S1 is well fitted by a power law with decay index $\delta_X = -1.6 \pm 0.35$ ($\chi^2 = 4.80$ for 8 d.o.f., 0.3–12 keV). This is somewhat lower than, but consistent with, the steep decay index $\delta_X = -3.0 \pm 1.9$ derived by Watson et al. (2002). The data quality of the corresponding co-added MOS1+2 lightcurve does not allow us to further constrain the fading

of S1. The decay of S1 is typical of X-ray afterglows having a decay index of $\delta_X \approx -1.4$ (Piro 2001). By extrapolating the best-fit pn lightcurve we predict the total number of counts in the second and third epoch *XMM-Newton* observations from S1 to be 0.04 counts and 0.02 counts, respectively (i.e., well below detectability). Hence, the second and third epoch observations establish that S1 is a non-persistent source; hence we identify S1 as the X-ray afterglow of GRB 001025A.

In order to compare the X-ray afterglow to the prompt X-ray emission as observed by the RXTE ASM we extracted the pn 1.5–12 keV lightcurve. A power law fit to the 1.5–12 keV light curve is not well constrained (decay index ~ -1). Hence, we extrapolated the best fit power law to the 0.3–12 keV light curve (renormalized to the 1.5–12 keV flux level) to the prompt emission phase. This extrapolation reproduces the RXTE ASM flux within the uncertainties (see Figure 6). However, fitting a power law to the fading of the prompt emission in the 1.5–12 keV band yields a steep power law (decay index -3.1 ± 0.4) underestimating the pn data points. Such a steep decay has been reported in several early X-ray afterglows observed with the *Swift* X-ray Telescope (Tagliaferri et al. 2003). It is not possible to fit a power law decay jointly to the fading prompt emission and the X-ray afterglow. The X-ray afterglow observed by *XMM-Newton* is therefore not a simple continuation of the prompt emission.

2.4.3. Spectral Analysis

Spectra of S1 were extracted from the first epoch observations and binned with a minimum of 20 counts per bin. Several spectral models were fitted to the pn and MOS1+2 spectra simultaneously: (i) power law models, representing synchrotron emission from a population of relativistic electrons in the fireball (Sari, Piran & Narayan 1998), (ii) thermal plasma emission giving rise to X-ray emission lines as seen in several other GRB afterglows (Reeves et al. 2002; Watson et al. 2003) (the MEKAL model as is typically used to represent thermal emission Mewe et al. 1985; Liedahl, Osterheld & Goldstein 1995), and (iii) combinations of (i) and (ii). In all models Galactic absorption was included, and additional absorption at the burst redshift was included in some of the models. A summary of the spectral fits is given in Tables 5,6,7 with errors quoted as 90% confidence intervals.

An absorbed synchrotron model is an acceptable fit to the spectrum (see Table 5), but the best-fit photon index is rather steep ($\Gamma \sim 2.8$, consistent with the findings of Watson et al. 2002). The Galactic H I column density in the direction of GRB 001025A is $6.1 \times 10^{20} \text{ cm}^{-2}$ and can in worst case be uncertain by up to 50% (Dickey & Lockman 1990). Power law models indicate absorption in excess of Galactic absorption, but the column density of extra-

galactic absorbing material is not strongly constrained. In this model the burst redshift is unconstrained.

An absorbed thermal plasma model (MEKAL) is as good a fit as the absorbed synchrotron emission model (see Table 6) and implies a plasma temperature around 3 keV and a burst redshift around $z \sim 0.3$. Watson et al. (2002) favor a redshift in the range 0.5–1.2 from their MEKAL model fits, and we note that the thermal plasma could be outflowing resulting in a host galaxy redshift lower by $\Delta z \sim 0.1$ (e.g. Reeves et al. 2002). Hence, thermal emission models do not provide strong constraints on the burst redshift. The absorbing column density at the burst redshift is at most twice the Galactic column density. The plasma abundances are not well constrained, but they are consistent with the solar values ($Z_{Fe} \lesssim 2Z_{\odot}$, $Z_{S,Si} \lesssim 13Z_{\odot}$).

Naturally, a model with a combination of a synchrotron emission component and a thermal emission component (see Figure 7) is also a good fit (see Table 7). The relative normalization of the synchrotron emission component and the thermal emission component is not well constrained, but the synchrotron emission component contributes $\sim 2/3$ of the total flux and above ~ 2 keV the synchrotron emission component dominates. The best-fit photon index is lower than in the pure synchrotron emission model fits ($\Gamma \sim 1.8$), but close to typical photon indices for X-ray afterglows (Piro 2001). The favored burst redshift is $z \approx 2$, and there is an indication of circumburst absorption ($N_H \sim 10 - 20 \times 10^{21} \text{ cm}^{-2}$). The abundances of the thermal plasma are not well constrained, but they are consistent with the solar values ($Z_{Fe,S,Si} \lesssim 6Z_{\odot}$).

In conclusion, an absorbed synchrotron model, an absorbed thermal plasma model, and a combination of the two all represent a good fit to the data. Consequently, we consider all these models in the following.

2.5. Spectral Energy Distribution

We derived the broadband spectral energy distribution by extrapolating the best-fit X-ray spectral models to the optical band. We used the X-ray decay index $\delta_X = -1.6$ to recast the X-ray spectrum to the epoch of the first R -band observations (1.20 days after the burst). For the synchrotron emission model (spectral index $\beta_X = 1.8$) an observed R -band extinction of at least 7 magnitudes is required to bring the model in agreement with the R -band upper limit (see Figure 8). On the other hand, extrapolating the synchrotron emission component from the best-fit combined synchrotron emission/thermal emission model (spectral index $\beta_X = 0.8$) to the R -band shows that the R -band upper limit is consistent with the model, if

the cooling break is close to the X-ray band.

3. DISCUSSION

The spectral index of the (X-ray) afterglow is a key parameter for constraining the properties of the burst and its environment. The pure synchrotron emission fit to the GRB 001025A X-ray afterglow has a very steep spectral index for a GRB X-ray afterglow. On the other hand, the synchrotron component of the combined thermal plasma/synchrotron model has a spectral index in line with what is found for other GRBs (Piro 2001). Detection of thermal afterglow emission has been reported in several other GRBs (see Watson et al. 2003, for an account of GRBs with thermal emission) increasing the soft X-ray flux in the $\sim 0.5 - 2$ keV range. One of the most prominent claims of thermal emission is in the GRB 011211 X-ray afterglow where thermal emission is detected during the first 5 ks of the *XMM-Newton* observation (Reeves et al. 2002). We investigated the effect on the spectral index of fitting an absorbed synchrotron model to a spectrum with thermal emission by fitting an absorbed synchrotron emission model to the first 5 ks of the GRB 011211 *XMM-Newton* spectrum. We obtain a spectral index of 1.6 ± 0.3 ; this is very similar to the spectral index ($\beta_X = 1.8 \pm 0.3$) we find fitting the same model to GRB 001025A. The steep spectral index of a pure synchrotron emission fit to GRB 001025A compared to the shallower index from a synchrotron emission plus thermal emission fit thus suggests that thermal emission may be steepening the X-ray afterglow spectrum of GRB 001025A.

Due to the different best fit spectral indices of the synchrotron emission in the pure synchrotron model and in the combined thermal plasma/synchrotron model, these two models have quite different implications for the deduced properties of the GRB 001025A fireball and its environment.

3.1. Physics of the Fireball

The prompt soft X-ray emission has a steep decay as seen in the tails of other GRBs (Smith et al. 2002; Giblin et al. 2002). Observations with the *Swift* XRT has revealed a population of bursts with an early steep decay and a shallower late time decay (Tagliaferri et al. 2003) similar to the behavior of GRB 001025A.

Several models predicts an early steep X-ray decay, including a hot cocoon surrounding a relativistic jet (Ramirez-Ruiz et al. 2002), emission from outside the relativistic beaming cone, $\theta > \Gamma^{-1}$, (Kumar & Panaitescu 2000), and a single spherical shell emitting instant-

neously (Fenimore et al. 1996). The steepness of the prompt emission decay excludes that the tail of the prompt emission is the onset of the afterglow (Sari, Piran & Narayan 1998). However, the afterglow could appear at any time > 16 s after the burst at which epoch the GRB 001025A afterglow is expected to be below the sensitivity of RXTE ASM.

The X-ray afterglow has a steep spectral index, if it is due to synchrotron emission only. The standard fireball model predicts in this case a temporal decay index of -2.2 ± 0.45 to -3.2 ± 0.45 for a spherical blast wave and an index of -3.6 ± 0.6 to -4.6 ± 0.6 for a jet (Zhang & Meszaros 2004). This is steeper than observed ($\delta_X = -1.6 \pm 0.35$), but only the jet model can be ruled out. If the X-ray afterglow is due to a combination of thermal plasma and synchrotron emission, the fireball model predicts a shallower afterglow decay index of the synchrotron component (index -0.4 ± 0.3 to -1.7 ± 0.9 for a spherical blast wave, index -1.9 ± 0.3 to -2.6 ± 1.2 for a jet, Zhang & Meszaros 2004) more in line with the X-ray lightcurve. In this case models where the X-ray afterglow originates from fast cooling are ruled out.

3.2. Burst Redshift and Luminosity

In the combined synchrotron/thermal plasma spectral model of the X-ray afterglow, the suggested burst redshift is $z \approx 2$. This yields an isotropic prompt energy release of 1.5×10^{53} erg (for a $H_0 = 72$ km/s/Mpc, $\Omega_m = 0.3$, $\Omega_\Lambda = 0.7$ cosmology) which is quite typical (e.g. Bloom, Frail & Kulkarni 2003). The isotropic 0.3–12 keV afterglow luminosity is $L_X = (3.2 \pm 2.6) \times 10^{45}$ erg/s time-averaged over the first *XMM-Newton* observation. We now compare the X-ray luminosity of GRB 001025A to the luminosities of the GRB sample of Berger et al. (2003). We use our derived X-ray afterglow decay index, flux and spectral index to calculate the isotropic luminosity ($L_{X,iso}$, eq. (1) in Berger et al. 2003, using their cosmology) of GRB 001025A 10 hours after the burst. In the combined synchrotron/thermal plasma model with a burst redshift $z = 2$, we find $L_{X,iso} = (2.4 \pm 1.9) \times 10^{46}$ erg/s. This is close to the typical X-ray afterglow luminosity at this epoch for the Berger et al. (2003) burst sample. However, in that sample, redshifts are not known for most of the bursts, in which case the luminosity has been derived assuming a redshift of $z = 1.1$. If GRB 001025A is at a redshift of $z = 1.1$ its isotropic luminosity is $L_{X,iso} = (3.5 \pm 2.5) \times 10^{45}$ erg/s which is in the low tail of the Berger et al. (2003) X-ray luminosity distribution. If the burst redshift is $z = 0.33$, as predicted in the thermal plasma only model, the luminosity of GRB 001025A $L_{X,iso} = (2.3 \pm 1.5) \times 10^{44}$ erg/s is lower than all GRBs in the Berger et al. (2003) sample.

The *B*-band detection of the likely host galaxy implies a redshift $z < 2.7$. The magnitude and color of the galaxy are consistent with a redshift around two, but they do not constitute

strong constraints on the redshift.

The pseudo-redshift estimate (Atteia 2003) for this burst $z = 0.8 \pm 0.4$, and although not strongly constraining, this is in line with the lower redshift derived from the thermal emission models of the X-ray afterglow.

3.3. The Burst Environment

The appearance of the candidate host galaxy is similar to other GRB hosts, i.e., an irregular morphology and a color that for a redshift of $z > 0.3$ is indicative of active star formation. From the absorbing column density in the soft X-ray band, the extinction towards the burst can be estimated by assuming a gas-to-dust ratio. The best-fit column densities at the burst redshift are $N_H \lesssim 20 \times 10^{21} \text{ cm}^{-2}$. Taking a Galactic gas-to-dust ratio (Predehl & Schmitt 1995), this translates into a restframe extinction of $A_V \lesssim 11$ for $z < 2$. Using an SMC gas-to-dust ratio results in $A_V \lesssim 1$, i.e. not enough to account for the extinction required in the pure synchrotron model for the X-ray afterglow. A Galactic gas-to-dust ratio is at variance with the findings for GRBs with detected optical afterglows generally having SMC-like gas-to-dust ratios (Galama & Wijers 2001). Either the pure synchrotron model is not appropriate for the GRB 001025A X-ray afterglow or GRB 001025A is much more obscured than bursts with detected optical afterglows (typically having $A_V \lesssim 0.2$ Hjorth et al. 2003a).

3.4. What Makes GRB 001025A a Dark Burst?

The dark bursts in the GRB sample of Jakobsson et al. (2004) (updated as of July 8, 2005, Jakobsson 2005) has a mean 1.6–10 keV flux of $3.0 \times 10^{-12} \text{ erg cm}^{-2} \text{ s}^{-1}$ 11 hours after the burst. Extrapolating the best-fit X-ray lightcurve of GRB 001025A to this epoch, the estimated 1.6–10 keV flux is $5.0 \pm 2.7 \times 10^{-13} \text{ erg cm}^{-2} \text{ s}^{-1}$. The X-ray afterglow of GRB 001025A is fainter than any of the dark bursts in the Jakobsson et al. (2004) sample and much fainter than the mean of GRBs with detected optical afterglows in this sample ($4.2 \times 10^{-12} \text{ erg cm}^{-2} \text{ s}^{-1}$).

The low R -band flux of GRB 001025A is not caused solely by a general faintness of the afterglow at all wavelengths. The R -band-to-3 keV spectral index is $\lesssim 0.43$ so GRB 001025A is clearly dark according to the definition of Jakobsson et al. (2004). For GRBs with detected optical afterglows, the R -band-to-3 keV spectral index is 0.73 and for *Swift* detected bursts it is 0.65 (Jakobsson 2005) so the afterglow of GRB 001025A is optically faint relative to

the X-ray band. The low optical-to-X-ray spectral index could be due to heavy obscuration in the burst environment. Alternatively, the cooling frequency could be close to the X-ray band, giving rise to a shallow spectral index requiring no optical obscuration.

The X-ray spectral index has been measured only for a few dark GRBs. By re-normalizing the X-ray spectrum and the optical observations to a common epoch (e.g. 11 h after the burst) and extrapolating the X-ray spectral index to the optical band, assuming a position of the cooling break, the R -band flux can be predicted. For three of the five GRBs with measured spectral index in the dark GRB sample of De Pasquale et al. (2003) (GRB 990704, GRB 990806, GRB 000214) the predicted R -band flux is lower than the observational upper limit, when invoking a cooling break at 1 keV. These three GRBs have steep X-ray spectral indices, possibly reflecting the presence of a thermal component on top of the synchrotron emission. The true synchrotron spectral index may thus be lower than the index obtained from a pure synchrotron emission fit, giving rise to even lower predictions for the optical flux. For the remaining two GRBs in the dark GRB sample of De Pasquale et al. (2003) (GRB 000210 and GRB 001109) obscuration is required in order to bring the observational upper limit in line with the model prediction (or the derived X-ray spectral index is too steep due to the presence of thermal emission). Two of the bursts detected by *Swift* and with published X-ray spectral index (GRB 050401 and GRB 050408, Chincarini et al. 2005) are dark according to the definition of Jakobsson et al. (2004). For both bursts obscuration is required in order to be consistent with the upper limit on the R -band flux, even when invoking a cooling break at 1 keV.

4. CONCLUSIONS

GRB 001025A was a long-duration GRB with a prompt emission spectrum well fitted by the Band model. The tail of the prompt soft X-ray emission decays too steeply to be the beginning of the afterglow. Three epoch *XMM-Newton* observations show that the GRB 001025A afterglow is X-ray faint. Furthermore, the optical flux is relatively low compared to the X-ray band. Either (i) the optical afterglow suffers extinction of at least seven magnitudes, or (ii) a significant fraction of the X-ray afterglow flux originates from a thermal plasma, and the cooling frequency is close to the X-ray band at 1.2 days after the burst. In the latter case, we predict that the burst redshift is around two, and we find that the X-ray luminosity and the spectral index are fairly typical of GRB afterglows. Alternatively, the GRB 001025A X-ray afterglow spectrum is characterized by a very steep synchrotron index, and GRB 001025A is situated in an environment with an unusually large gas-to-dust ratio, consistent with the Galactic ratio.

The present study of GRB 001025A, and the properties of the few other dark GRBs with measured spectral index, raises the possibility that some bursts appear optically dark because their afterglow is faint, and their cooling frequency is close to the X-ray band. The viability of this scenario can be tested from early observations of X-ray afterglows from dark GRBs yielding the temporal and spectral behaviour of the X-ray afterglows, which in turn constrain the geometry of the blast wave and the underlying physical processes. This would provide a crucial test for physical differences between dark bursts and bursts with an optical afterglow.

We are grateful to Dale Frail for making the results of his VLA observations known to us. We thank the anonymous referee for useful and very detailed comments that improved the presentation of our results. KH is grateful for *Ulysses* support under JPL Contract 958056, for support from the Long Term Space Astrophysics program under NAG5-3500, and for support as a Participating Scientist in the NEAR mission under NAG5-9503. KP and JPUF acknowledge support from the Carlsberg foundation. KP acknowledges support from Instrument Center for Danish Astrophysics. PJ acknowledges support from a special grant from the Icelandic Research Council. This work was supported by the Danish Natural Science Research Council (SNF). From the Russian side this work was supported by the Russian Space Agency contract and RBRF grant 03-02-17517. DAS is supported by an NSF Astronomy and Astrophysics Postdoctoral Fellowship under award AST-0105221. The authors acknowledge benefits from collaboration within the EU FP5 Research Training Network "Gamma-Ray Bursts: An Enigma and a Tool". Based on observations obtained with *XMM-Newton*, an ESA science mission with instruments and contributions directly funded by ESA Member States and NASA, and based on observations made with ESO Telescopes at the La Silla or Paranal Observatories under programme 66.A.-0386(A).

Facilities: XMM(EPIC), VLT(ANTU), RXTE(ASM), NEAR(XGRS), Wind(Konus).

REFERENCES

- Altieri, B., Schartel, N., Santos, M., Tomas, L., Guainazzi, M., Piro, L., & Parmar, A. 2000a, GCN Circ. 869 (<http://gcn.gsfc.nasa.gov/gcn/gcn3/869.gcn3>)
- Altieri, B., Schartel, N., Lumb, D., Piro, L., & Parmar, A. 2000b, GCN Circ. 884 (<http://gcn.gsfc.nasa.gov/gcn/gcn3/884.gcn3>)
- Atteia, J.-L. 2003, A&A 407, L1
- Band, D., et al. 1993, ApJ 413, 281

- Berger, E., et al. 2002, ApJ 581, 981
- Berger, E., Kulkarni, S.R., Frail, D.A., 2003, ApJ 590, 379
- Berger, E., et al. 2005, ApJ submitted, astro-ph/0505107
- Bloom, J.S., Frail, D.A. & Kulkarni, S.R. 2003, ApJ 594, 674
- Bloom, J.S., et al. 2005, ApJ submitted (astro-ph/0505480)
- Castro Cerón, J.M., et al. 2004, A&A 424, 833
- Costa, E., 1999, A&AS 138, 425
- Chincarini, G. et al. 2005, astro-ph/0506453
- Crew, G. et al. 2003, ApJ 599, 387
- De Pasquale, M. et al., 2003, ApJ 592, 1018
- Dickey, J.M. & Lockman, F.J., 1990, ARA&A, 28, 215
- Djorgovski, S.G., et al. 2001, ApJ 562, 654
- Fenimore, E.E., et al. 1996, ApJ 473, 998
- Fynbo, J. P. U., et al. 2000, GCN Circ. 867 (<http://gcn.gsfc.nasa.gov/gcn/gcn3/867.gcn3>)
- Fynbo, J. P. U., et al. 2001, A&A 369, 373
- Galama, T.J. & Wijers, R.A.M.J. 2001, ApJ 549, L209
- Gehrels, N., et al. 2005, Nature submitted (astro-ph/0505630)
- Giblin, T.W., et al. 2002, ApJ 570, 573 A&A 383, 112
- Gorosabel, J., et al. 2002, A&A 383, 112
- Groot, P., et al. 1998, ApJ 493, L27
- Hjorth, J., et al. 2002, ApJ 576, 113
- Hjorth, J., et al. 2003a, ApJ 597, 699
- Hjorth, J., et al. 2003b, Nature 423, 847
- Hjorth, J., et al. 2005, ApJ submitted (astro-ph/0506123)

- Hurley, K., Cline, T., & Smith, D. 2000, GCN Circ. 863
(<http://gcn.gsfc.nasa.gov/gcn/gcn3/863.gcn3>)
- Hurley, K. 2000, GCN Circ. 864, (<http://gcn.gsfc.nasa.gov/gcn/gcn3/864.gcn3>)
- Hurley, K. et al. 2002, ApJ 567, 447
- Jakobsson, P. et al. 2004, ApJ 617, L21
- Jakobsson, P. 2005, <http://www.astro.ku.dk/~pallja/dark.html>
- Kumar, P., & Panaitescu, A. 2000, ApJ 541, L51
- Lamb, D.Q., & Reichart, D. 2000, ApJ 536, 1
- Lazatti, D., Covino, S., & Ghisellini, G., 2002, MNRAS 330, 583
- Liedahl, D.A., Osterheld, A.L., & Goldstein, W.H., 1995, ApJ 438, L115
- Malesani, D., et al. 2004, ApJ 609, L5
- Meszáros, P. 2002, ARAA 40, 137
- Mewe, R., Gronenschild, E.H.B.M., & van den Oord, G.H.J., 1985, A&AS 62, 197
- Piro, L., 2001, in Gamma-ray bursts in the afterglow era, eds. E Costa, F. Frontera, & J. Hjorth (Springer - Berlin), p. 97
- Piro, L., et al., 2002, ApJ 577, 680
- Predehl, P. & Schmitt, J.H.M.M., 1995, A&A 293, 889
- Preece, R., Pendleton, G., Briggs, M., Mallozzi, R., Paciesas, W., Band, D., Matteson, J., & Meegan, C. 1998, ApJ 496, 849
- Ramirez-Ruiz, E., et al., 2002, MNRAS 337, 1349
- Reichart, D., & Price, P. 2002, ApJ 565, 174
- Rol, E. et al. 2005, accepted for publication in ApJ
- Reeves, J. et al. 2002, Nature 416, 512
- Sari R., Piran, T. & Narayan, R., 1998, ApJ 497, L17
- Schlegel, D.J. et al. 1998, ApJ 500, 525

- Smith, D.A., Levine, A., Remillard, R., Hurley, K., & Cline, T. 2000, GCN Circ. 861
(<http://gcn.gsfc.nasa.gov/gcn/gcn3/861.gcn3>)
- Smith D.A., et al., 2002, ApJS 141, 415
- Stanek, K.Z., et al., 2003, ApJ 591, L17
- Tagliaferri, G., et al., Nature accepted, astro-ph/0506355
- Taylor, G.B., et al., 1998, ApJ 502, L115
- Uemura, M., Kato, T., Ishioka, R., Iwamatsu, H., & Yamaoka, H. 2000 GCN Circ. 866
(<http://gcn.gsfc.nasa.gov/gcn/gcn3/866.gcn3>)
- Watson, D., Reeves, J., Osborne, J., O'Brien, P., Pounds, K., Tedds, J., Santos-Lleo, M., & Ehle, M. 2002 A&A 393, L1
- Watson, D., Reeves, J., Hjorth, J., & Pedersen, K. 2003 ApJ 595, L29
- Zhang, B. & Meszaros, P. 2004 Int. J. Mod. Phys. A 19, 2385

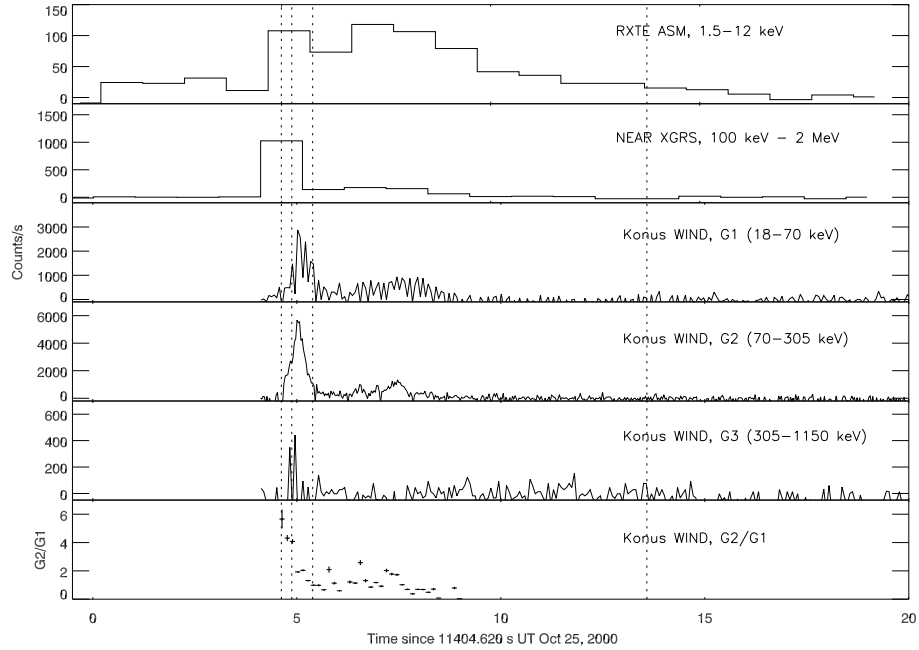


Fig. 1.— Lightcurves of GRB 001025A. Plotted from top to bottom are the background subtracted lightcurves of RXTE ASM (1.5–12 keV, 1 s resolution), NEAR XGRS (100 keV–2 MeV, 1 s resolution), *Wind-Konus* in three different energy bands (18–70 keV, 70–305 keV, 305–1150 keV, 0.128 s resolution), and the hardness ratio between the *Wind-Konus* 70–305 keV and 18–70 keV energy bands as function of time. The vertical dotted lines indicate the intervals where time-resolved spectroscopy was done, see Fig 2.

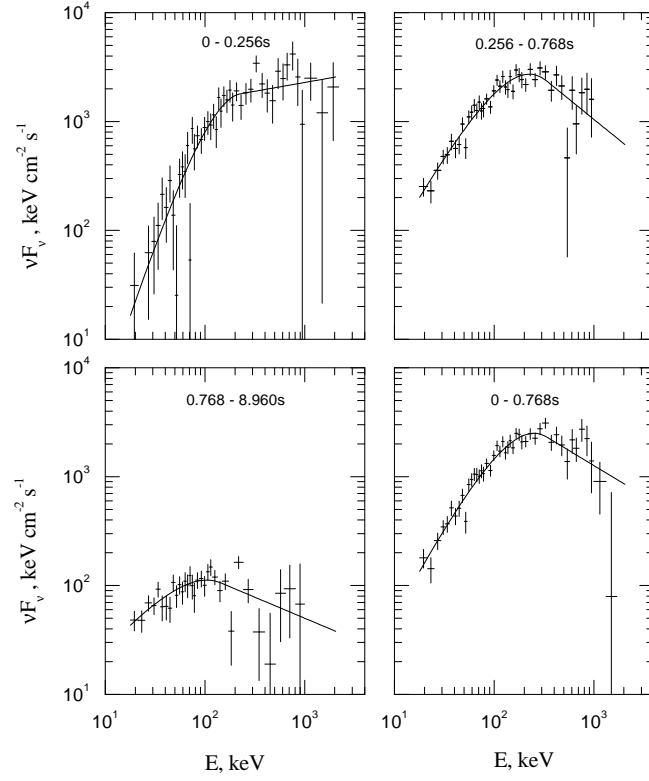


Fig. 2.— Time-resolved energy spectra of GRB 001025A in νF_ν units from *Wind-Konus*. Spectral fitting was done using the Band model. The fitting parameters are given in Table 2. The time intervals used for the spectral fits are indicated in Figure 1.

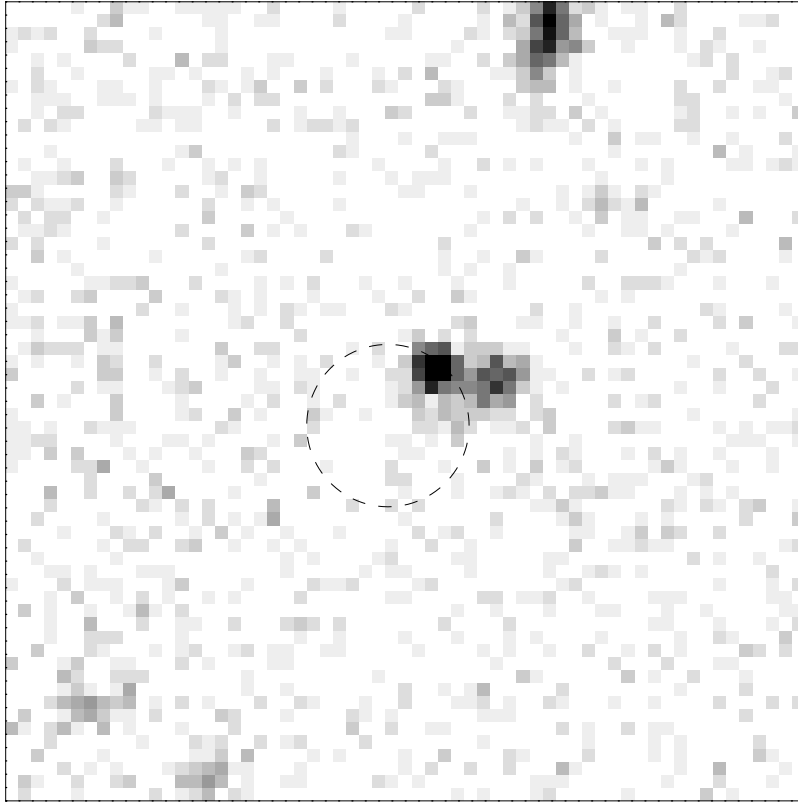


Fig. 3.— 12×12 arcsec² VLT *R*-band image with the 2σ error circle of source S1. North is up and East is to the left.

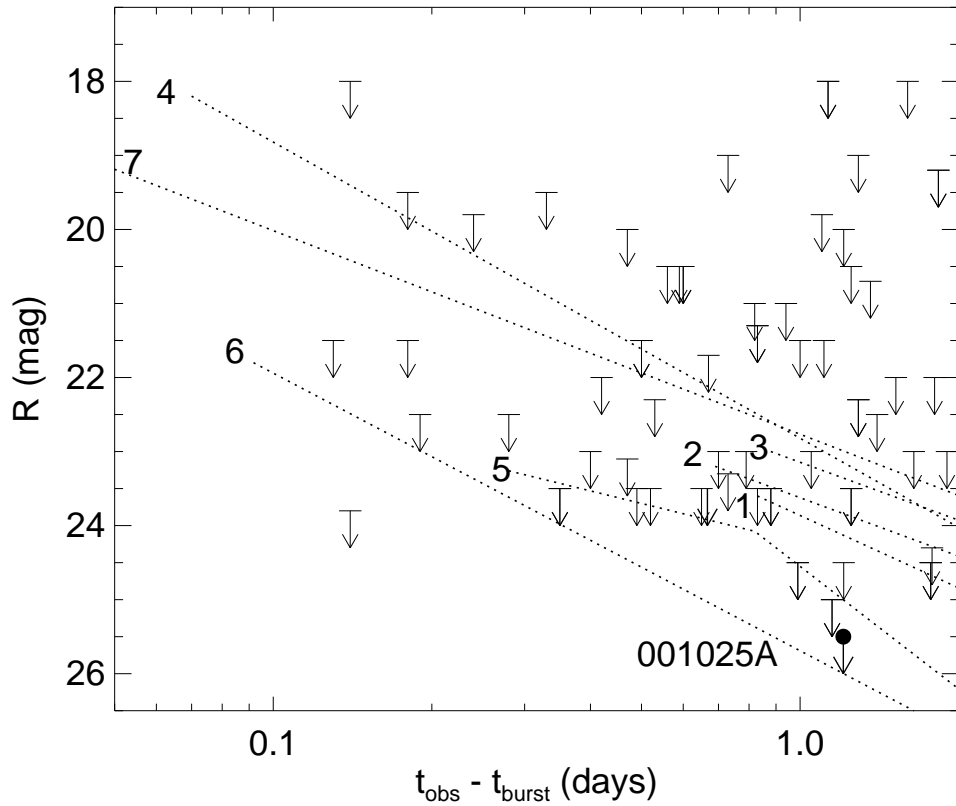


Fig. 4.— R -band magnitudes and upper limits as a function of time for various gamma-ray bursts in the pre-*Swift* era, compared to the observations of GRB 001025A (filled circle). The dotted lines sketch the decay of optically dim bursts, starting at the time of the first observation. The labels are as follows: (1) GRB 980329, (2) GRB 980613, (3) GRB 000630, (4) GRB 020124, (5) GRB 020322, (6) GRB 030115, (7) GRB 021211.

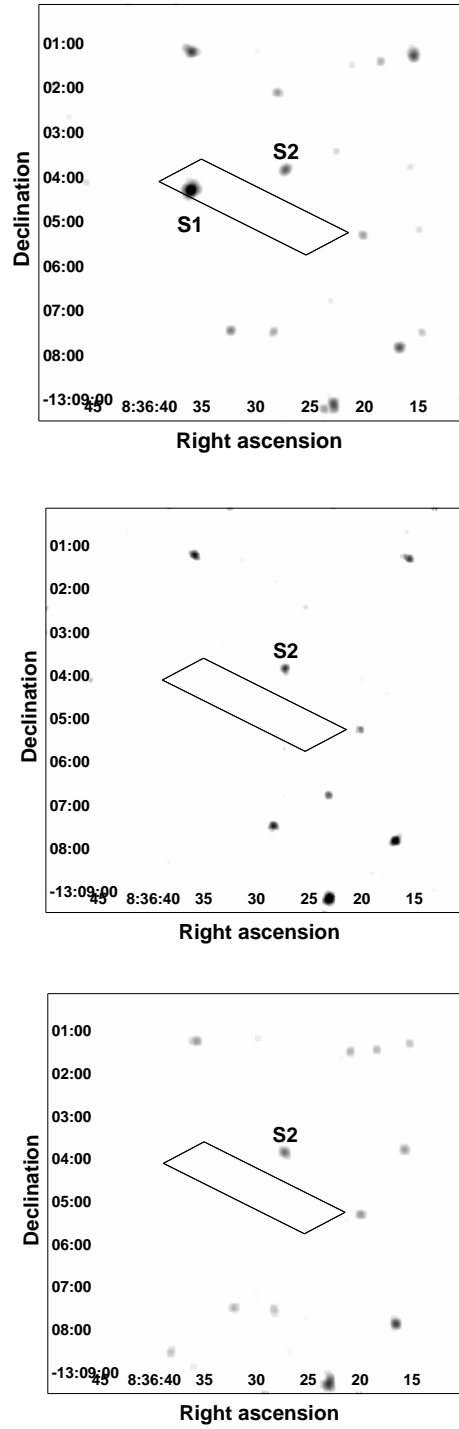


Fig. 5.— *XMM-Newton* co-added pn+MOS1+MOS2 images showing the afterglow, S1, and the source S2, with the final RXTE-ASM/IPN error box overlaid, at three epochs: Top: 1.88 days after the burst. Middle: 761 days after the burst. Bottom: 910 days after the burst. See Table 4 for the exposure time of individual images.

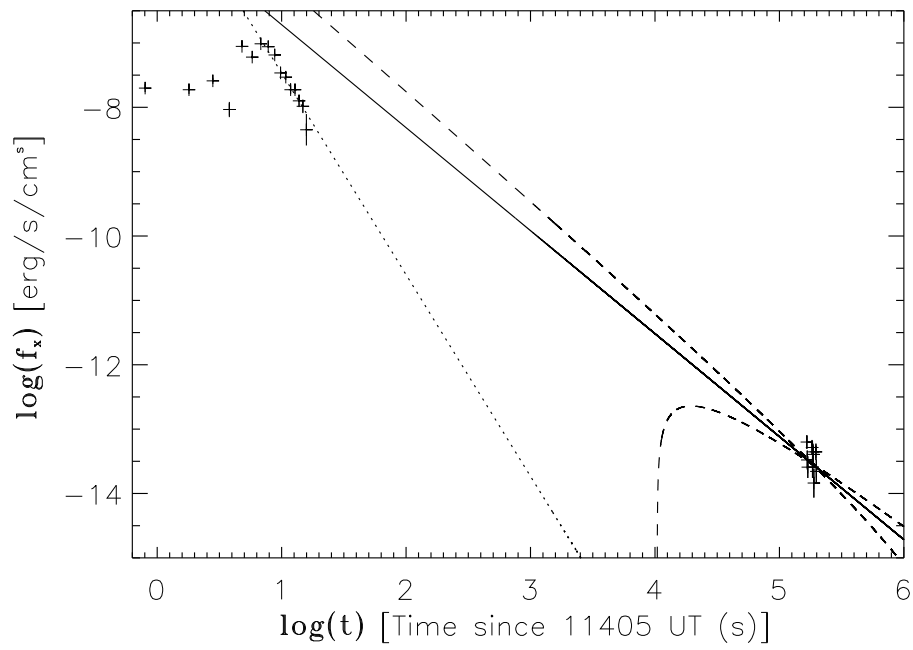


Fig. 6.— RXTE ASM and *XMM-Newton* pn 1.5–12 keV lightcurves with power law fits overlaid. Dotted line: Fit to the tail of the RXTE ASM lightcurve. Full line: Fit to *XMM-Newton* pn 0.3–12 keV lightcurve renormalized to the 1.5–12 keV flux level. Dashed lines: 1σ envelope of fit to *XMM-Newton* pn 0.3–12 keV lightcurve renormalized to the 1.5–12 keV flux level.

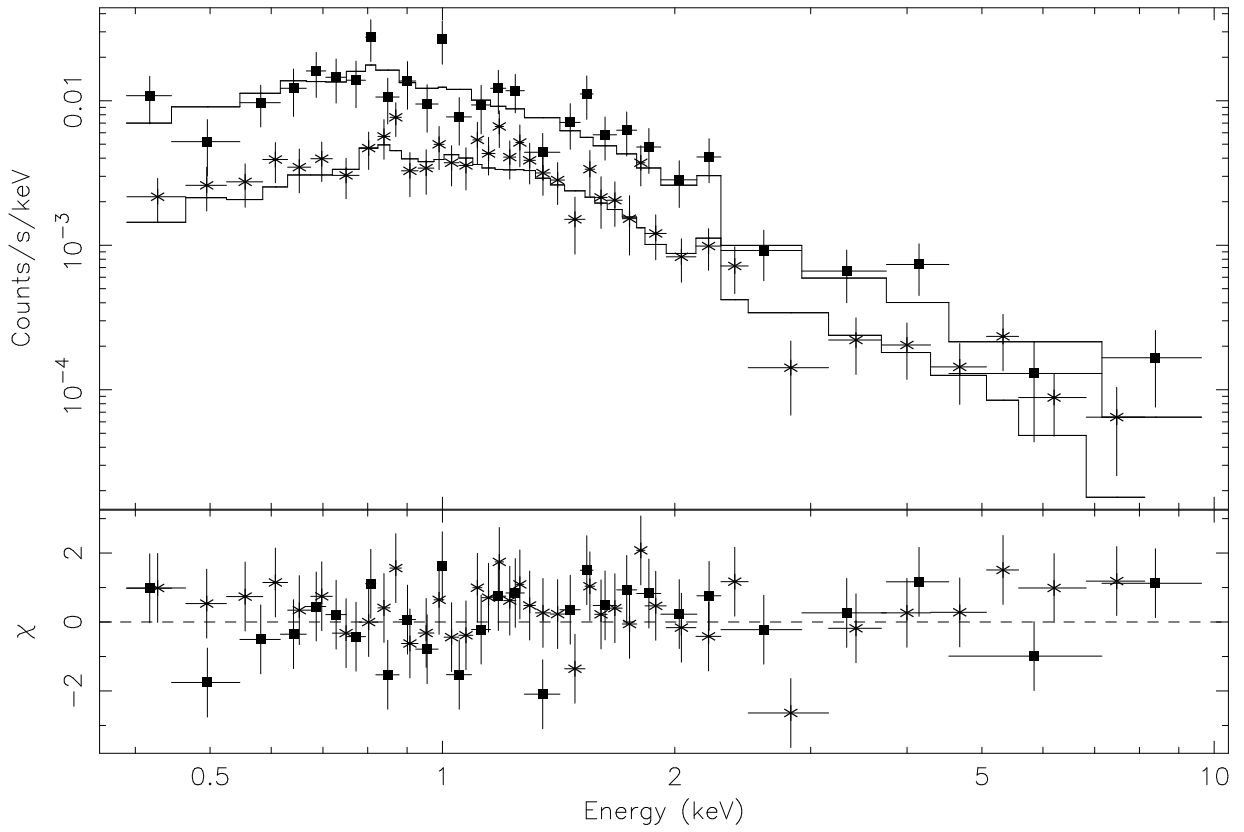


Fig. 7.— Top panel: *XMM-Newton* pn (squares) and MOS1+2 (stars) spectra of the afterglow of GRB 001025A with a spectral binning of min. 10 counts per bin. Overplotted is the best-fit combined synchrotron/thermal emission model with fixed Galactic absorption and absorption at the burst redshift. Lower panel: residuals of model fit.

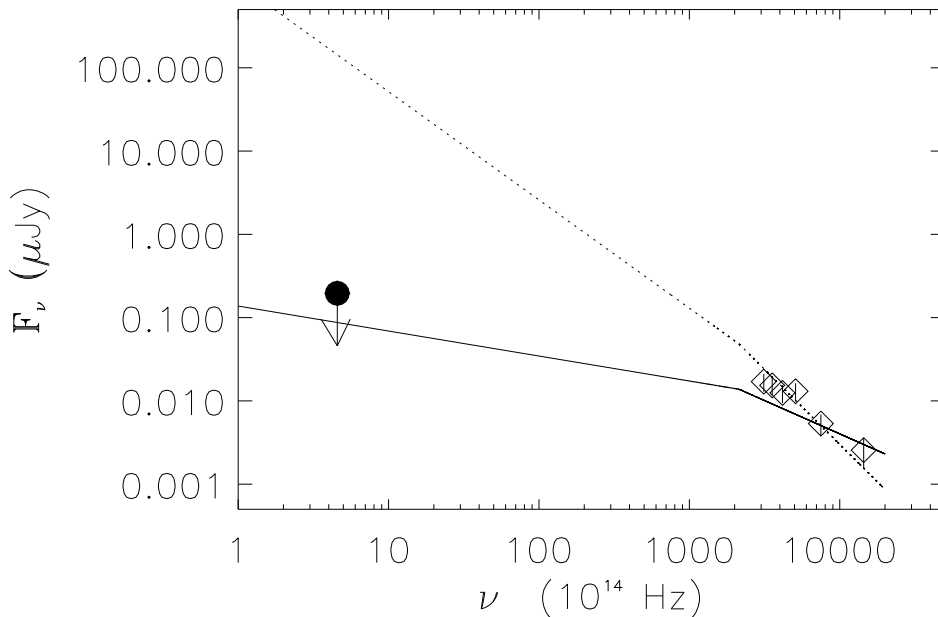


Fig. 8.— The optical to X-ray spectral energy distribution of GRB 001025A 1.20 days after the burst. The *XMM-Newton* pn spectrum recast to this epoch is shown as diamonds (only data points above 1.3 keV, where absorption is negligible), the *R*-band upper limit is shown as the filled circle. Overlaid is the synchrotron emission component of the best-fit from the combined synchrotron emission/thermal emission model (spectral index 0.8, full line) and the best-fit synchrotron emission model (spectral index 1.8, dotted line). The extrapolation to the optical band assumes that the cooling break is at 1 keV (2140×10^{14} Hz) and that the spectral index changes by -0.5 (Sari, Piran & Narayan 1998) when going to the short frequency side of the break.

Table 1. *Corners of the final ASM-IPN Error Box for GRB 001025A*

R.A.(2000)	decl.(2000)
129°1456	–13°0579
129°1619	–13°0663
129°0891	–13°0854
129°1054	–13°0938

Table 2. *Spectral Fits to the Prompt Emission of GRB 001025A^a*

Interval (s)	Normalization (photons cm ⁻² s ⁻¹)	α	β	E ₀ (keV)
0–0.256	0.26 ± 0.1	+0.81 ± 0.57	-1.84 ± 0.12	85 ± 33
0.256–0.768	0.37 ± 0.04	-0.39 ± 0.11	-2.75 ± 0.2	140 ± 19
0.768–8.960	0.03 ± 0.1	-0.99 ± 0.3	-2.40 ± 0.2	103 ± 46
0–0.768	0.29 ± 0.04	-0.30 ± 0.12	-2.55 ± 0.16	148 ± 20
0–8.960	0.036 ± 0.004	-0.91 ± 0.1	-2.40 ± 0.16	191 ± 37

^aNote: See Eq. 1 for the definition of α , β , and E₀.

Table 3. *Journal of VLT Observations*

UT	Δt (days)	Filter	Exp. time (s)	Seeing (arcsec)
2000 Oct 26.34	1.21	<i>R</i>	12×200	0.50–0.75
2000 Oct 27.32	2.19	<i>R</i>	8×200	0.50–0.75
2001 Mar 23.02	146.89	<i>B</i>	3×200	0.45–0.55
2001 Mar 23.04	146.91	<i>R</i>	10×200	0.45–0.55

Table 4. *XMM-Newton Observations of GRB 001025A*

Date ^a	Time since GRB (days)	Instrument	Exposure time ^b (ks)
2000 Oct 27.003 ^c	1.88	pn	15
		MOS	32
2002 Nov 25.16 ^d	761	pn	8.8
		MOS	8.6
2003 Apr 23.29 ^e	910	pn	18
		MOS	19

^aStart of observation

^bExposure time for each detector used in the analysis, i.e. with high background periods left out

^cTarget of opportunity observation (Altieri et al. 2000a,b)

^dAO-2 observation

^eContinuation of AO-2 observation

Table 5. *Synchrotron Model Fits to the X-ray Afterglow Spectrum of GRB 001025A*

Model	Γ^a	Absorption ^b (10^{21} cm^{-2})	Redshift ^c	$\chi^2/\text{d.o.f.}$
Fixed index, fixed Galactic abs.	2.0	0.61	0	66.8/33
Free Galactic abs.	2.8 ± 0.3	$2.6_{-0.6}^{+0.4}$	0	32.6/32
Fixed Galactic abs, free abs. at z	2.6 ± 0.3	15_{-5}^{+26}	< 7.5	31.3/31

^aPhoton index.

^bColumn density of absorber at the quoted redshift.

^cRedshift of absorber.

Table 6. *Thermal Emission Model Fits to the X-ray Afterglow Spectrum of GRB 001025A*

Model	T (keV)	Absorption ^a (10 ²¹ cm ⁻²)	Redshift ^b	χ^2 /d.o.f.
Fixed Gal. abs.	3.0 ^{+0.5} _{-0.4}	0.61	0.32 ± 0.05	36.7/32
Free Gal. abs.	2.8 ± 0.4	0.9 ^{+0.4} _{-0.3}	0.33 ± 0.05	34.1/31
Fixed Gal. abs, free abs. at z	2.8 ± 0.5	0.5 ^{+0.7} _{-0.5}	0.33 ± 0.05	33.7/31

^aAbsorber column density.

^bCommon redshift of thermal emission and extra-galactic absorber.

Table 7. *Combined Synchrotron Model and Thermal Emission Model Fits to the X-ray Afterglow Spectrum of GRB 001025A*

Model	Γ^a	T (keV)	Absorption ^b (10^{21} cm^{-2})	Redshift ^c	$\chi^2/\text{d.o.f.}$
Fixed index, free Gal. abs.	2.0	1.5 ± 0.6	$3.0_{-1.0}^{+1.4}$	$1.98_{-0.15}^{+0.13}$	17.9/27
Fixed Gal. abs.	$1.2_{-1.5}^{+1.6}$	$2.8_{-0.7}^{+0.5}$	0.61	0.32 ± 0.05	34.1/29
Free Gal. abs.	$1.9_{-0.4}^{+0.6}$	$1.6_{-0.4}^{+0.5}$	$2.8_{-0.7}^{+1.0}$	$2.00_{-0.15}^{+0.12}$	18.4/28
Fixed Gal. abs, free abs. at z	1.8 ± 0.6	1.8 ± 0.6	17_{-6}^{+9}	2.00 ± 0.13	19.6/28
Fixed index, free abs. at z	2.0	1.7 ± 0.5	17 ± 6	$2.00_{-0.14}^{+0.12}$	19.8/29

^aPhoton index.

^bAbsorber column density.

^cCommon redshift of thermal emission and extra-galactic absorber.